Electronic Supplementary Material (ESI) for Inorganic Chemistry Frontiers.

Supporting information

Cyanamide defects induced built-in electric field in crystalline carbon nitride for enhanced visible to near infrared light photocatalytic activity

Jinyu Zhu,[a] Guoqiang Zhang,[a] Yangsen Xu,*[b] Wei Huang,[a] Chuanxin He,[a] Peixin Zhang,[a] Hongwei Mi*[a]

[a] College of Chemistry and Environmental Engineering, Shenzhen University, Shenzhen, Guangdong, 518060, PR China. E-mail: milia807@szu.edu.cn (H. Mi).

[b] Institute of Information Technology, Shenzhen Institute of Information Technology, Shenzhen, Guangdong, 518172, PR China. E-mail: xuys2008@163.com (Y. Xu)

1. Experimental Section

1.1 Characterizations

The Brunauer-Emmett-Teller (BET) specific surface area and pore size distribution is measured using an ASAP 2460 automatic specific surface area and porosity analyser, through the liquid N_2 adsorption-desorption process. The UV-vis diffuse reflectance absorption is recorded with a UV-3600PLUS scanning spectrophotometer, under a two beam optical system composed of 50 W halogen lamp and deuterium lamp (Jindao, Japan). The inductively coupled plasma (ICP) spectrometry is performed on Ultima 2, Horiba. The X-ray photoelectron spectrum (XPS) analyses are conducted on the K-Alpha$^+$ model with the monochromatic X-ray photoelectron spectrometer (Thermo Fisher Scientific, Britain). The fluorescence emission spectra are recorded on the F7000 fluorescence spectrometer (Hitachi). The time-resolved fluorescence spectra are analysed on an Edinburgh instruments FS5 fluorescence spectrometer. The field emission scanning electron microscope (FESEM) images are performed on a SU8010. The transmission electron microscope (TEM) images are executed

under JEM-2100 & X-Max80 operated at 200 kV (Japan Electronics, Japan). The crystalline structure is characterized by an X-ray diffractometer (XRD) (Empyrean), using Cu $K_{\square}$ radiation (λ = 1.54056 A). The Fourier transform infrared (FTIR) spectra are recorded on a Nicolet iz10 spectrometer. The Kelvin probe force microscopy (KPFM) measurement are conducted with the atomic force microscope (Dimension Icon, Bruker, Germany). The Raman measurement is excited under visible light at 620 nm with a Leica microscope from German (inVia, Renishaw, Britain). The electron paramagnetic resonance (EPR) was operated under low temperature (77 K, BrukerA300).

1.2 The linear sweep voltammetry (LSV) measurements

The KCCN, KSCN 1.0 and KOCN 0.5 materials loaded with Pt were prepared through 1 mL H_2PtCl_6 and 50 mg KCCN, KSCN 1.0 and KOCN 0.5 powder, respectively, under full optical spectrum for 0.5 h. The test solution system was consisted with 1 mL H_2PtCl_6, 10 mg amples, 40 μL Nafion and had it ultrasonic for 2h. Then, 6μL solution is dropped on ring glassy carbon electrode and dried under infrared light. The measurement system is operated with three electrodes system with glassy carbon electrode as working electrode, Ag/AgCl as counter electrode, platinum tablet as reference electrode. The activating CV measurement is performed under Triethanolamine electrolyte with 20 mV scan speed under electrochemical window of 0 to -2 V, the LSV test of KCCN, KSCN 1.0, KOCN 0.5, Pt-KCCN, Pt-KSCN 1.0, Pt-KOCN 0.5 was conducted after stable CV scanning.

1.3 Photocatalytic H_2 production

The 50 mg of samples added with H_2PtCl_6 (3wt% Pt) is placed into a 50 mL of TEOA solution (10vol%) in a closed gas circulation system (Beijing Perfectlight, Labsolar-6A). The irradiations of visible-light, later region of visible light and near infrared light is obtained from the 300 W Xe lamp (Beijing Perfectlight, PLS-SXE300) respectively allocated with a UVCUT-420 filter, UVCUT-500 filter and UVCUT-700 filter. All tests are controlled at 5 ℃ by circulating condensate, in the vacuum environment. The evolved gases are detected *in-situ* by using an online gas chromatograph (GC9790II, Fuli) equipped with a thermal conductivity detector (TCD).

1.4 AQE calculations of H_2 production

The 100 mg of KSCN 1.0 added with H_2PtCl_6 (3wt% Pt) is placed into a 100 mL of TEOA solution (10vol%) with 3wt% KCl in a closed gas circulation system. The catalyst solution is irradiated by a 300W Xe lamp applying bandpass filters (center at 420, 450, 475, 500 nm) for 1 h , after the photocatalytic reduction for half an hour without any filters. All tests are controlled at 25 ℃ by circulating condensate. The average intensity of irradiation is determined by an FZ-A spectroradiometer (Photoelectric Instrument Factory of Beijing Normal University). The apparent quantum efficiency (AQE) was calculated from equation:

$$AQE = \frac{2 \times the\ number\ of\ evolved\ H_2\ molecules}{the\ number\ of\ incident\ photons} \times 100\%$$

1.5 Photocurrent measurement

The 10 mg of samples is dispersed in a 100 mL of 0.2 mg/mL I_2/acetone solution under ultrasonic treatment. A two-electrode process is used to deposit the samples at the applied potential of 30 V for 5 min. FTO glass substrates with the coated area about 1 × 3 cm^2 is used for both electrodes. Then, the deposited electrode is dried at 200 °C for 30 min to remove I_2 residues. An FTO photoanode deposited samples, Hg/$HgCl_2$, and Pt foil electrode acts as the working electrode, reference electrode and counter electrode, respectively. A 0.5 M of Na_2SO_3 aqueous solution is used as the electrolyte. The photoanode is illuminated by a 300 W Xe lamp with a UVCUT-420 nm filter.

2. Computation Section

The density functional theory (DFT) calculations were performed with the VASP package. Zero damping D3 correction method of Grimme was used to describe van der Waals interactions. Built to the vacuum layer spacing was set to 15 Å along the *z* direction to avoid interactions between periodic images. The generalized gradient approximation (GGA) of Perdew−Burke−Ernzerhof (PBE) was used to calculate exchange-correlation energies, where the force-, energy-convergence criterion for self-consistent field (SCF), and energy cutoff were set to 1 × 10^{-5} eV, 0.05 eV $Å^{-1}$, and 450 eV, respectively. A Monkhorst−Pack (3 × 3 × 1) *k*-point grid was employed for faster convergence during optimization.

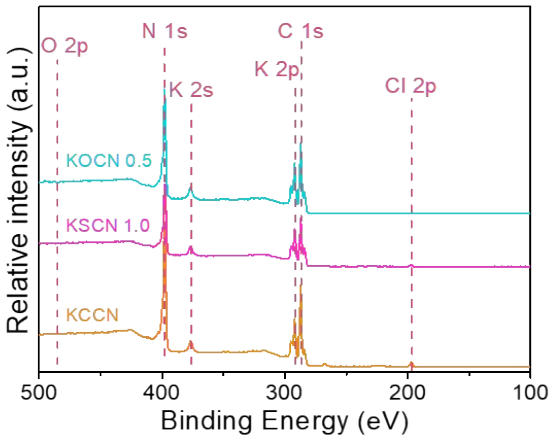

Fig. S1. The XPS survey spectrum of KCCN, KSCN 1.0 and KOCN 0.5.

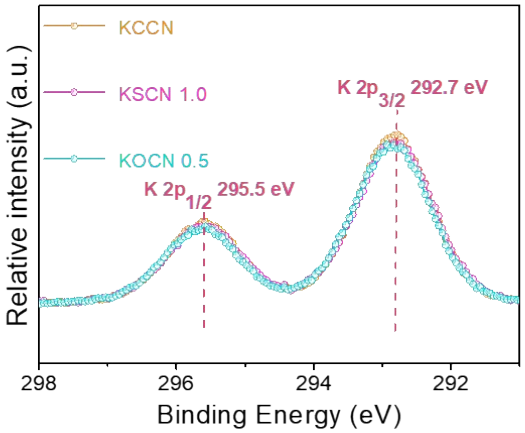

Figs. S2. The K 2p XPS of KCCN, KSCN 1.0 and KOCN 0.5.

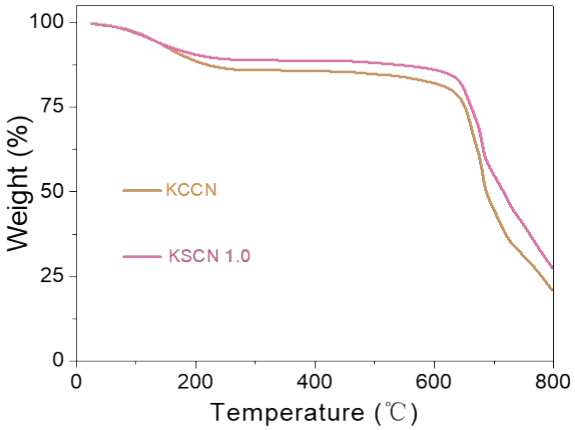

Fig. S3. The thermogravimetry curves of KCCN and KSCN 1.0.

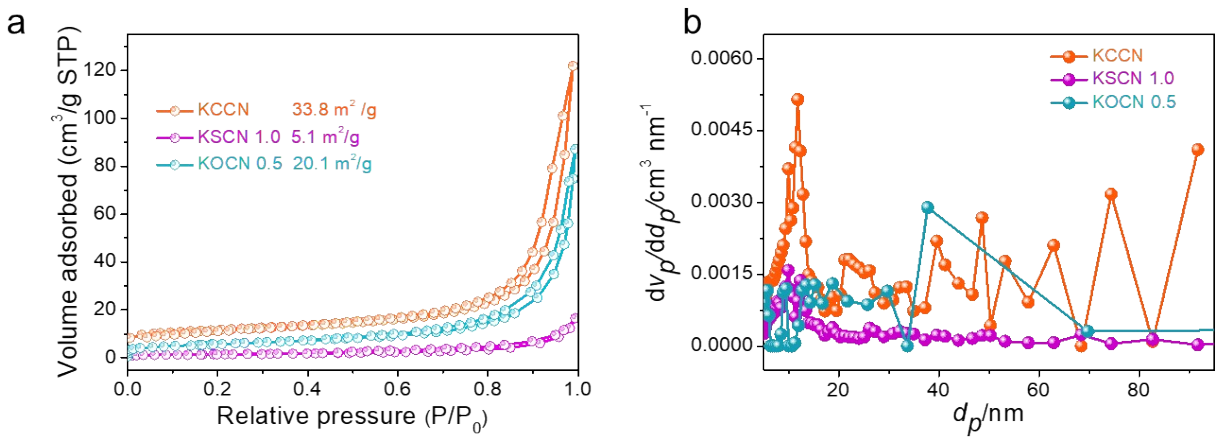

Fig. S4. The BET isothermal curves (a) and the pore size distribution curves (b) of KCCN, KSCN 1.0 and KOCN 0.5, respectively.

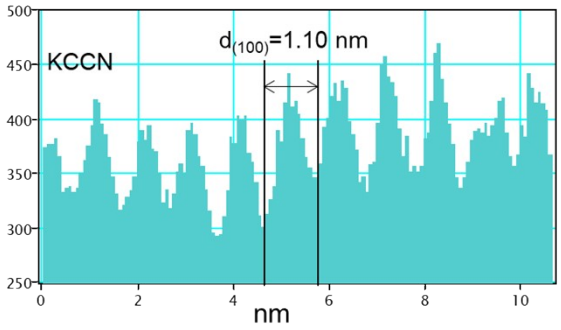

Fig. S5. The lattice fringes profile of KCCN along the white line inserted in KCCN HR-TEM image.

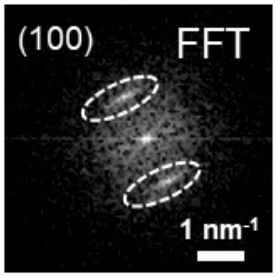

Fig. S6. The fast Fourier transform (FFT) pattern from the HR-TEM image of KCCN.

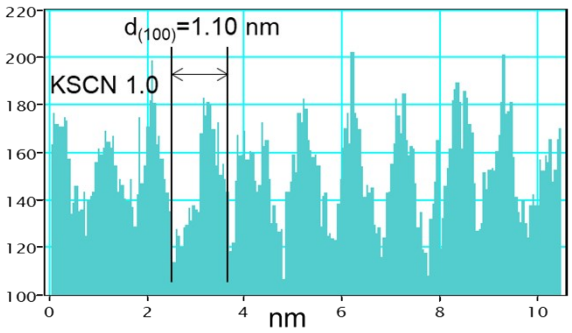

Fig. S7. The lattice fringes profile of KSCN 1.0 along the white line inserted in KSCN 1.0 HR-TEM image.

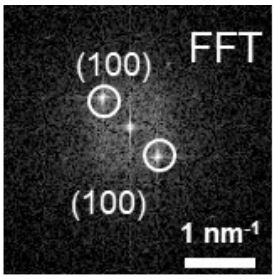

Fig. S8. The fast Fourier transform (FFT) pattern from the HR-TEM image of KSCN 1.0.

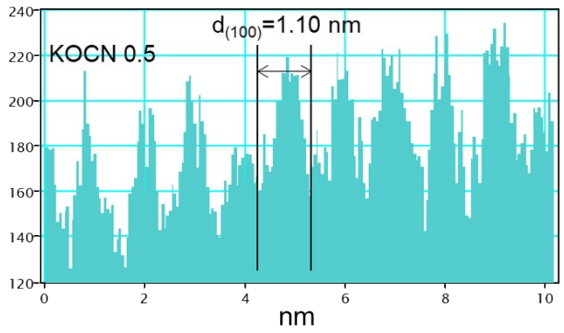

Fig. S9. The lattice fringes profile of KOCN 0.5 along the white line inserted in KOCN 0.5 HR-TEM image.

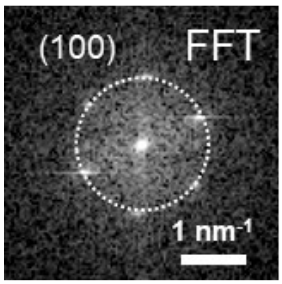

Fig. S10. The fast Fourier transform (FFT) pattern from the HR-TEM image of KOCN 0.5.

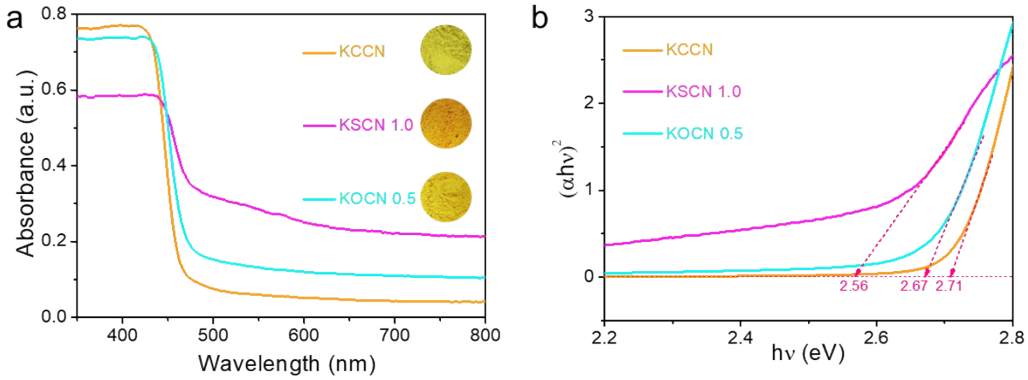

Fig. S11. The solid UV-vis diffuse reflection spectra (DRS) (a) and the Tauc plot transform analysis graph (b) of KCCN, KSCN 1.0 and KOCN 0.5, respectively.

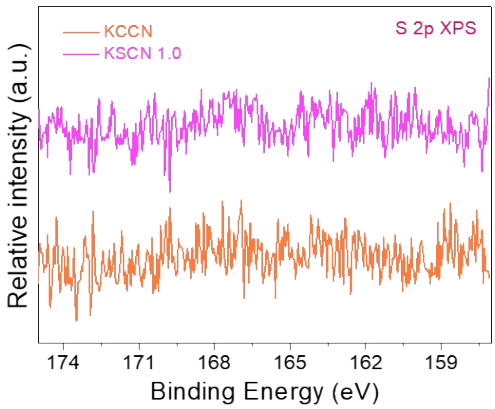

Fig. S12. The S 2p XPS spectra of KCCN and KSCN 1.0.

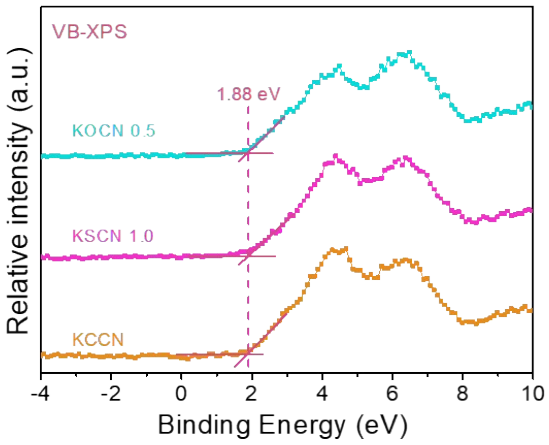

Fig. S13. The valence band (VB) XPS spectra of KCCN, KSCN 1.0 and KOCN 0.5.

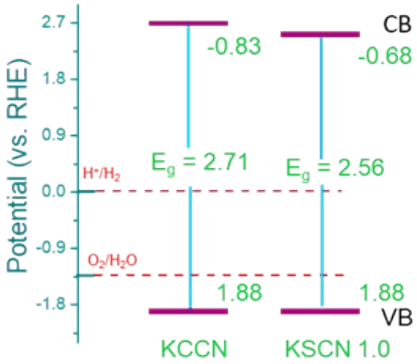

Fig. S14. The energy band layout of KCCN, KSCN 1.0.

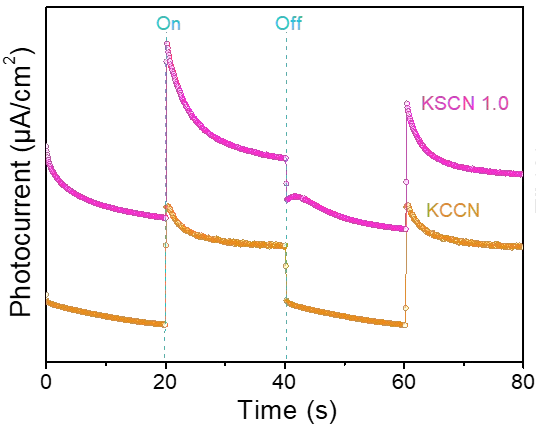

Fig. S15. The photocurrent spectra of KCCN and KSCN 1.0.

Fig. S16. The electrochemical impedance spectroscopy (EIS) spectra of KCCN and KSCN 1.0.

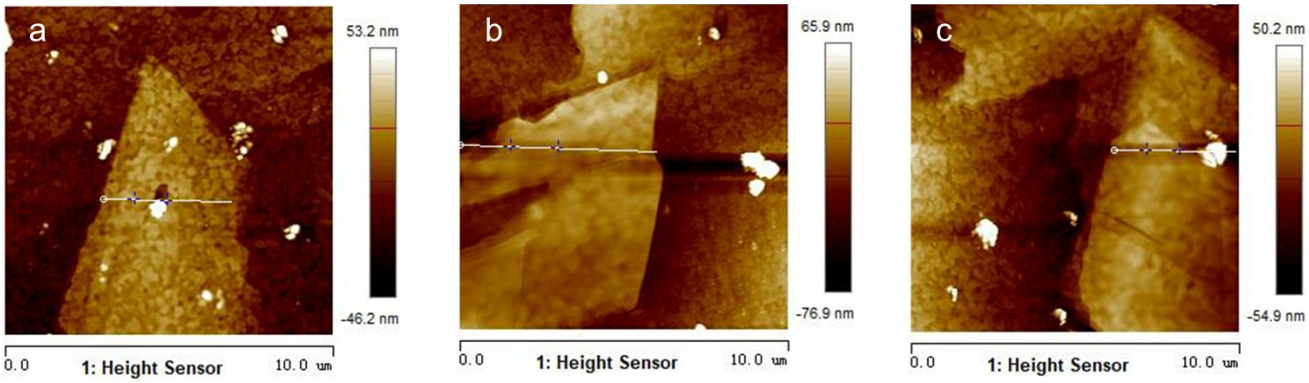

Fig. S17. The images of AFM morphology of KCCN (a), KSCN 1.0 (b) and KOCN 0.5 (c), respectively.

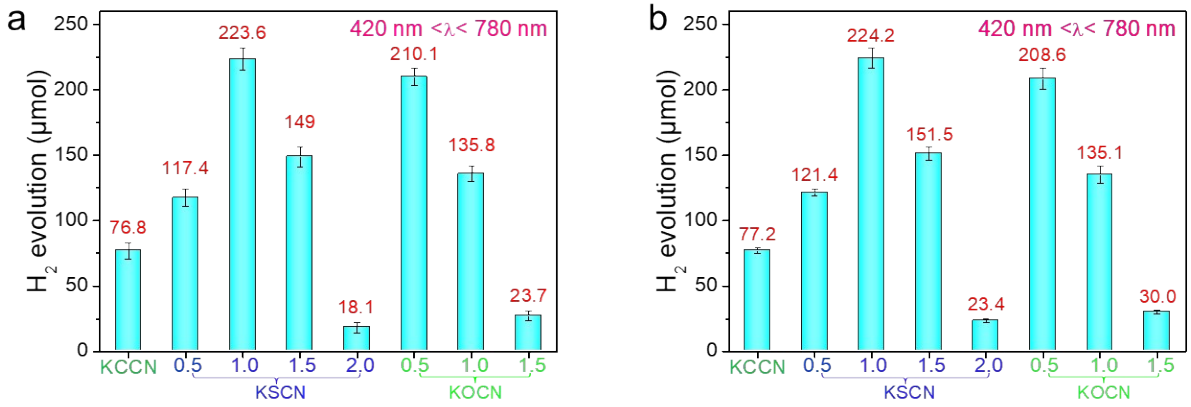

Fig. S18. The parallel experiments (a-b) of H_2 evolution results of KCCN, KSCN*x* (*x* = 0.5, 1.0, 1.5, 2.0) and KOCN*x* (*x* = 0.5, 1.0, 1.5) under irradiation of 420 nm <λ< 780 nm.

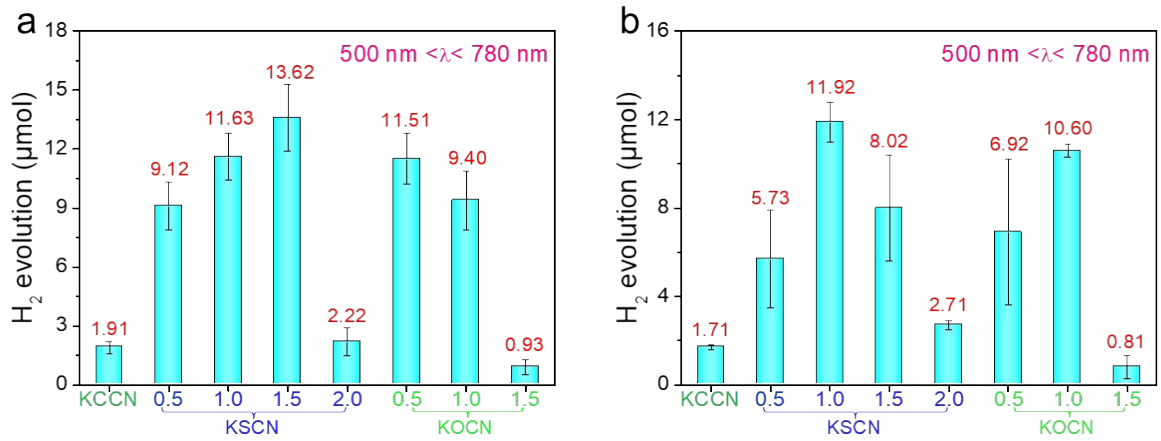

Fig. S19. The parallel experiments (a-b) of H_2 evolution results of KCCN, KSCN*x* (*x* = 0.5, 1.0, 1.5, 2.0) and KOCN*x* (*x* = 0.5, 1.0, 1.5) under irradiation of 500 nm <λ< 780 nm.

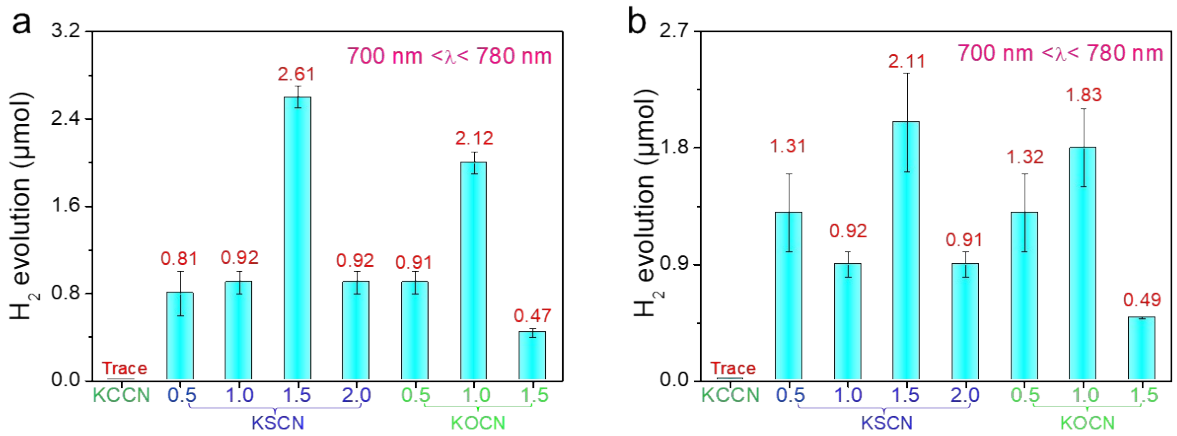

Fig. S20. The parallel experiments (a-b) of H_2 evolution results of KCCN, KSCN*x* (*x* = 0.5, 1.0, 1.5, 2.0) and KOCN*x* (*x* = 0.5, 1.0, 1.5) under irradiation of 700 nm <λ< 780 nm.

As shown in Fig. S18, the best H_2 evolution rate was uniformly around 2.9 and 2.7 times over KSCN 1.0 and KOCN 0.5 to KCCN in two parallel experiments，respectively under 420 nm < λ <780 nm irritation. The parallel experiments' performance performed under the 500 nm < λ <780 nm was similarly around 7 and 6 times from KCCN-cya to KCCN materials, respectively (Fig. S19). Moreover, the identically activated activity produced under 700 nm < λ <780 nm was identically exhibited in the parallel experiments (Fig. S20).

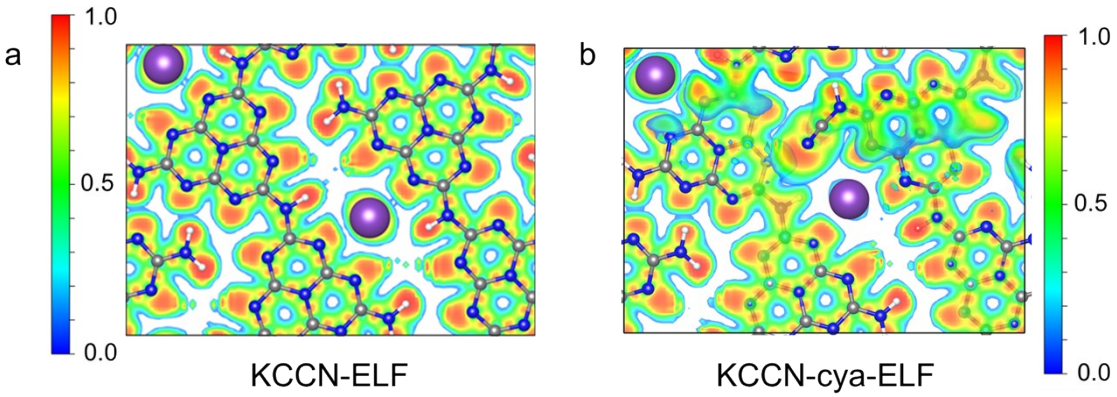

Fig. S21. The electron localization function (ELF) patterns of KCCN (a) and KCCN-cya (b), respectively.

Table S1. The element analysis table (EA) of KCCN and KSCN 1.0

Elemental analysis	KCCN	KSCN 1.0
C (wt%)	25.82	26.08
N (wt%)	42.97	43.41
H (wt%)	1.628	1.701
C/N (mol ratio)	0.669	0.701

Table S2. The inductively coupled plasma (ICP) measurement table of K element over KCCN and KSCN 1.0.

ICP	KCCN	KSCN 1.0
K (wt%)	11.2	11.7

Table S3. The analysis data of transient photoluminescence test of KCCN, KSCN 1.0 and KOCN 0.5.

	τ_1 (ns)	τ_2 (ns)	a_1	a_2	$\tau_{average}$ (ns)
KCCN	1.23	14.45	249.29	1.60	2.16
KSCN 1.0	1.10	4.56	216.03	11.20	1.71
KOCN 0.5	1.04	4.28	192.40	8.41	1.54

Table S4. The cyano group peak area from Fourier transform infrared spectra and the corresponding H_2 evolution rates of KCCN, KSCN *x* (*x* = 0.5, 1.0, 1.5, 2.0, 3.0), respectively.

Sample	KCCN	KSCN 0.5	KSCN 1.0	KSCN 1.5	KSCN 2.0	KSCN 3.0
Area of cyano group	10.49	20.84	44.38	45.67	100.12	210.16